Diagnosed Characteristics of Precipitation Systems over Taiwan during the May–June 1987 TAMEX

RICHARD H. JOHNSON AND JAMES F. BRESCH

Department of Atmospheric Science, Colorado State University, Fort Collins, Colorado

(Manuscript received 10 May 1990, in final form 8 October 1990)

ABSTRACT

Characteristics of Mei-Yu precipitating cloud systems over Taiwan during the May–June 1987 Taiwan Area Mesoscale Experiment (TAMEX) have been studied using sounding, surface precipitation, and radar data. Vertical motion has been computed over the island at 6-h intervals from 13 May to 15 June using a modification of the kinematic method that takes into account the mountainous lower boundary within a four-station sounding polygon.

Two primary characteristics of the precipitation have been found. First, the major rainfall events were linked to the passage of midlatitude disturbances and typically consisted of both deep convective and stratiform components. Deep convection was primarily prefrontal or frontal, while the stratiform precipitation was postfrontal, presumably in association with overrunning and orographic lifting. Second, there was a pronounced diurnal variability in the rainfall.

Vertical motion, heating (Q_1), and moistening (Q_2) profiles have been used to define the character of the precipitating systems. During periods of deep convection (as indicated by radar and surface rainfall measurements), a separation of the Q_1 and Q_2 peaks is observed, whereas at times of stratiform precipitation, the Q_1 and Q_2 peaks are nearly coincident. The findings for Taiwan generally support those of Luo and Yanai, indicating a predominance of stratiform rainfall over the entire southern China and Yangtze regions (including Taiwan) during the Mei-Yu; however, they also suggest that in at least a portion of this region (Taiwan), precipitation may consist of a mixture of deep convective and stratiform components. The occurrence of coincident Q_1 and Q_2 peaks in the mid- to lower troposphere (600–800 mb) during moderate-to-heavy stratiform rain events indicates the importance of shallow cold-frontal and/or stable orographic lifting. Thus, it appears that in the Taiwan area, heavy rain in stable situations may depend critically on low-level forcing mechanisms.

The evolution of the sea breeze, the development of the afternoon mixed layer, and the diurnal cycle of Q_1 and Q_2 have been examined on a synoptically undisturbed day (24 May) when afternoon thunderstorms occurred over Taiwan. Moistening of the boundary layer by the daytime sea breeze was evident. A high-level heating peak and a midtropospheric drying peak were observed in the afternoon in association with the sea breeze and deep convection. In the evening, heating and drying aloft and cooling and moistening at low levels occurred, suggestive of stratiform precipitation during the decaying stage of the convection.

1. Introduction

The period of May through June marks the transition in east Asia from the northern monsoon to the southern monsoon and is characterized by a quasi-stationary frontal zone that frequently produces heavy rainfall over southern China, Taiwan, and the Yangtze Valley. Rainfall in this latter region is referred to as the Mei-Yu. While there have been considerable studies of Mei-Yu precipitation systems (Tao and Chen 1987), the detailed mechanisms of heavy rain production over Taiwan are not well known. The May–June 1987 Taiwan Area Mesoscale Experiment (TAMEX) was designed to investigate the processes that produce heavy rain over Taiwan during the Mei-Yu season (Kuo and Chen 1990).

In a previous study, Luo and Yanai (1983, 1984) computed precipitation, vertical motion, heating (Q_1) and moistening (Q_2) distributions over the Yangtze and southern China regions (including the Taiwan area). They showed through an analysis of the Q_1 and Q_2 profiles that much of the Mei-Yu rainfall is produced through large-scale or stratiform precipitation processes. It is of interest to know to what extent their conclusions can apply to precipitation systems occurring locally over the Taiwan area. In order to determine the general character of the cloud systems producing rainfall over Taiwan, we will compute the vertical motion and the heating and moistening distributions within these systems using 6-h sounding data from the TAMEX special observing period (SOP; mid-May to mid-June). We will then relate these computed fields to the precipitation structure of the cloud systems as determined by TAMEX research radars.

Corresponding author address: Dr. Richard H. Johnson, Dept. of Atmospheric Science, Colorado State University, Fort Collins, CO 80523.

Diurnal variations in precipitation on Taiwan are particularly noteworthy, with the diurnal behavior principally being determined by sea and land breezes and their interactions with the prevailing low-level monsoon flow. These effects on tropical and subtropical islands have been studied for many years (Leopold 1949; Malkus 1955). In the Asian monsoon area, the diurnal cycle of convection as influenced by sea and land breezes has been documented in the vicinity of Borneo by Houze et al. (1981) and Johnson and Priegnitz (1981). Convergence of the land breeze and the northeast winter monsoon flow over the South China Sea appears to generate offshore convection along the north coast of Borneo at night, while during the daytime a precipitation maximum assisted by the sea breeze shifts to land. Observations from TAMEX suggest a similar diurnal variation of precipitation on Taiwan. It will be seen, however, that while a diurnal signal is generally evident throughout TAMEX, it is often contaminated by other effects (e.g., fronts, convection, cloud cover, etc.).

In this paper we examine the diurnal cycle in precipitation over Taiwan both 1) from a broad perspective for the entire SOP and 2) in detail for a synoptically undisturbed, 3-day period of TAMEX (24–26 May) when afternoon convection occurred over the interior. Emphasis in the latter case will be given to the boundary-layer structure of the sea breeze in order to better understand the generation of the afternoon convection over the interior. TAMEX offers a unique opportunity to investigate the diurnal cycle on Taiwan since it provides the first four-per-day sounding dataset for any continuous, extended period on the island.

The format of the paper will be to first examine the pattern of precipitation and vertical motion for the entire SOP (mid-May to mid-June). Two primary heavy rainfall episodes occurred during this period, one on 17–18 May (referred to as intensive observing period or IOP 2) and the other on 7–8 June (IOP 8). Radar-determined precipitation characteristics, vertical motion, and heating and moistening distributions during the two episodes will be presented. Finally, the detailed characteristics of the sea and land breezes and vertical motion for the undisturbed period 24–26 May will be documented.

2. Data analysis and procedures

Upper-air and rainfall data were obtained from the United States TAMEX Data Management Center. Six-hourly soundings were available from a mesoscale network during the SOP. Four of the sounding sites—Panchiao, Hualien, Tung Kang, and Makung—were used to outline a polygon around Taiwan (Fig. 1). Data from these sites were subjected to gross error checks. Time–height cross sections of winds were then used to find and correct vertical inconsistencies. Seven missing soundings were replaced by linear interpolation of soundings launched 6 h before and after the missing

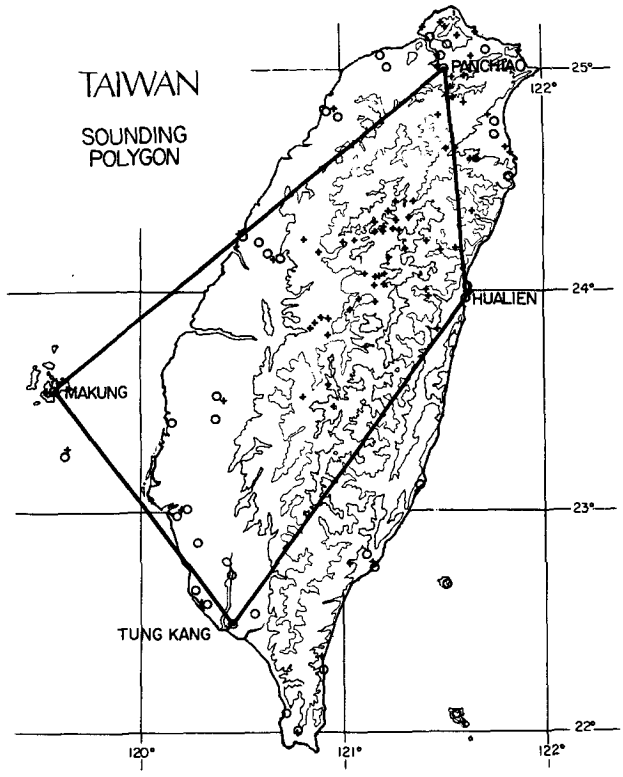

FIG. 1. Sounding polygon comprising Panchiao, Hualien, Tung Kang, and Makung. Topographic contours are at 100, 500, and 2500 m. Open circles are weather reporting stations and pluses indicate hourly precipitation stations.

time. Moisture data from Hualien were at times found to have a physically unrealistic vertical profile, normally characterized by thin, exceptionally dry layers. The relative humidity RH in such layers (identified by RH $< 30\%$) was replaced by averaged values from immediately adjacent levels. The corrected sounding data were then interpolated to 25-mb levels from the surface to 100 mb.

Because Taiwan's central mountain range, with elevations extending above 3000 m, occupies a substantial portion of the polygon area, a modification of the standard kinematic vertical-velocity calculation method is required. Nitta (1983) developed a method for calculating the vertical p-velocity ω over Tibet, which accounted for the atmospheric displacement by the Plateau. This approach has been adapted for Taiwan as follows: the area of the polygon was divided into a fractional atmospheric area, $\sigma_a(p)$, and a fractional mountain area, $\sigma_m(p)$. The vertical velocity within σ_a, denoted as $\bar{\omega}$, can be found from the continuity equation

$$\overline{\nabla \cdot \mathbf{V}} + \frac{\partial \sigma_a \bar{\omega}}{\partial_p} = 0, \qquad (1)$$

where $\overline{\nabla \cdot \mathbf{V}}$ is the divergence over the entire polygon calculated using the line integral method. The area oc-

cupied by mountains as a function of pressure was obtained on each 25-mb level by subjective determination from a topographic map. This topographic correction adjusts $\bar{\omega}$ only below 700 mb (i.e., where $\sigma_a < 1$). The vertical motion and divergence profiles were also adjusted following the procedure of O'Brien (1970), and $\bar{\omega}$ is assumed to be zero at sea level and 100 mb.

Another topographic correction was applied when computing the line integral for the divergence calculation. It can be seen from Fig. 1 that two sides of the polygon, from Tung Kang to Hualien and from Hualien to Panchiao, transect the mountains. A topographic cross section from Tung Kang to Hualien is shown in Fig. 2. Below mountaintop levels, winds at each pressure level are assumed to be constant from the station to the mountainside, as opposed to the customary assumption of a linear variation between stations. The wind is set to zero where the pressure surface is below ground and in the narrow mountain valleys. Sensitivity tests indicate that the latter assumption, based on reasonable estimates of valley winds, has only a minor (<10%) effect on results.

The apparent heat source Q_1 and the apparent water vapor sink Q_2 have been computed as follows:

$$Q_1 = \sigma_a \frac{\partial \bar{T}}{\partial t} + \overline{\overline{\mathbf{V}\cdot\nabla T}} + \frac{\bar{\omega}}{\pi}\frac{\partial \bar{\theta}}{\partial p} \tag{2}$$

$$Q_2 = -\frac{L}{c_p}\left(\sigma_a \frac{\partial \bar{q}}{\partial t} + \overline{\overline{\mathbf{V}\cdot\nabla q}} + \bar{\omega}\frac{\partial \bar{q}}{\partial p}\right), \tag{3}$$

where $\pi = (1000/p)^{\kappa}$; $\kappa = R/c_p$; and $\bar{T}$, $\bar{q}$, and $\bar{\theta}$ are the average temperature, mixing ratio, and potential temperature over the polygon. The advection terms (e.g., $\overline{\overline{\mathbf{V}\cdot\nabla q}}$) were calculated using

$$\overline{\overline{\mathbf{V}\cdot\nabla q}} = \overline{\overline{\nabla\cdot\mathbf{V}\,q}} - \bar{q}\,\overline{\overline{\nabla\cdot\mathbf{V}}}, \tag{4}$$

where $\overline{\overline{\nabla\cdot\mathbf{V}\,q}}$ was computed analytically using the approach of Molinari and Skubis (1988).

In order to examine conditional instability, vertical profiles of saturation moist static energy h^* were calculated using

$$h^* = c_pT + gz + Lq^*, \tag{5}$$

where z is the geopotential height and $*$ indicates saturation values.

Fifty-six hourly rainfall stations (comprised of Central Weather Bureau and Taiwan Power Company stations; Fig. 1) were used to obtain polygon area rainfall for the purpose of calibrating the integrated heat and moisture budgets (Yanai et al. 1973). Hourly data for the *entire* SOP (the period of interest in this study) were limited to this network of unevenly distributed stations. In order to obtain a reasonable estimate of area-averaged rainfall for such an uneven distribution of stations, the polygon area was divided into eighteen 0.5° × 0.5° grid boxes. Grid-box average rainfall was

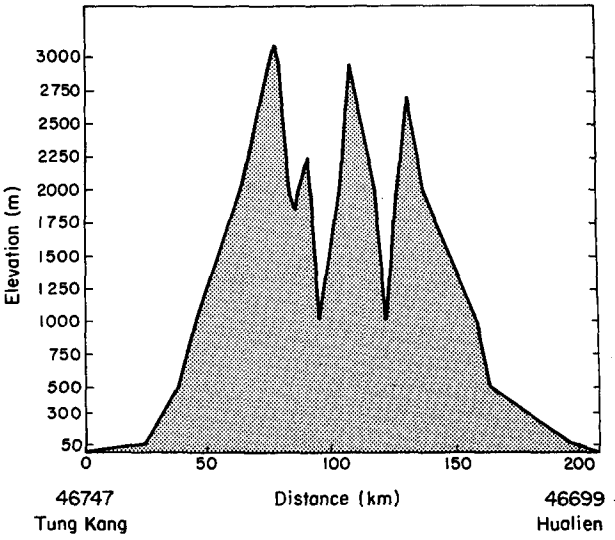

FIG. 2. Topographic cross section from Tung Kang to Hualien used in vertical motion computation. Vertical scale is greatly exaggerated.

calculated and an area-weighted polygon rain was obtained from

$$\bar{R} = \frac{1}{A}\sum_{i=1}^{18} \epsilon_i \bar{r}_i, \tag{6}$$

where $\bar{R}$ is the average polygon rainfall, A is the total area of the polygon, ϵ_i is the fraction of a grid-box area that lies within the polygon, and $\bar{r}_i$ is the average of the hourly rain from all stations within the ith box.

While the above procedure provides useful information concerning area-averaged rainfall, two of the 0.5° grids in the southwestern part of the polygon contain no stations. For these grids we have averaged data from neighboring grid boxes. While this situation is not ideal, it is a reasonable approach given the available *hourly* rainfall data. Comparison of time series of mountain and west coastal plain rainfall using the hourly rainfall data with that derived from a very dense network of *daily* rainfall stations (596 total) gave very close agreement. This comparison lends confidence to our rainfall analyses despite the inadequate spatial coverage of the hourly rainfall stations.

3. Precipitation, vertical motion, and heat and moisture budget results

a. Special observing period (13 May–15 June)

1) PRECIPITATION

A precipitation record for the entire SOP is illustrated in Fig. 3. Here we used 1-h data from the 56 stations in Fig. 1 to determine 6-h totals (centered at the four synoptic times, 0000, 0600, 1200, and 1800 UTC, which correspond to 0800, 1400, 2000, and 0200 LST, respectively) in two subdivisions: the mountains and

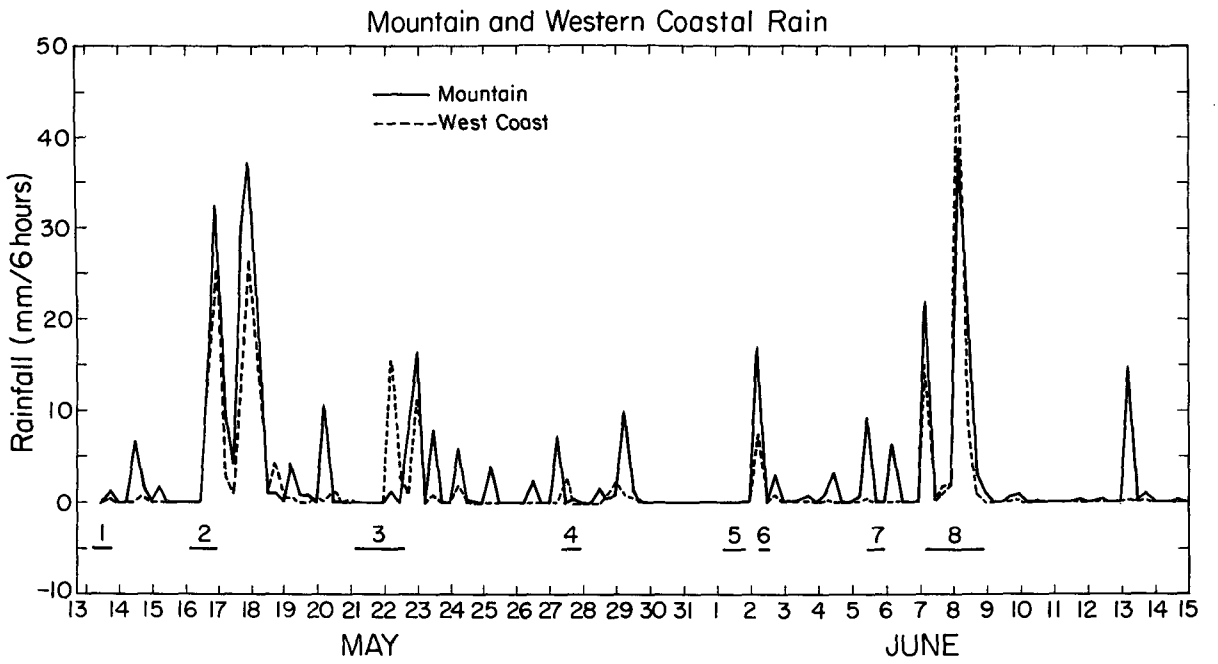

FIG. 3. Rainfall time series [mm (6 h)$^{-1}$] for the mountain area and the western coastal plain during the special observing period. Eight intensive observing periods (IOPs) are indicated at the bottom. Tick marks on abscissa correspond to 1200 LST.

the west coastal plain. The mountain domain corresponds to most locations in the polygon above 0.5 km and the coastal plain to all of the polygon area to the west. The rain rates in each domain in Fig. 3 are for the same unit area.

Several features are evident from the rainfall time series. First, there were two major periods of heavy rainfall, one around 17–18 May (IOP 2) and another on 7–8 June (IOP 8). Both episodes consisted of two peaks separated by 24 h. The first peaks were characterized by prefrontal deep convective rainfall (including a squall line with trailing stratiform precipitation in the May case; Wang et al. 1990) and the second by mostly frontal and postfrontal stratiform precipitation (Parsons and Trier 1989; Trier et al. 1990). Radar data for these cases will be presented later. It is interesting to note here, however, that the second periods, those consisting of predominantly stratiform rain, yielded the greatest areal-averaged precipitation amounts. In both the May and June cases, heavy rainfall occurred both in the mountains and on the western coastal plains.

A second prominent feature of Fig. 3 is a pronounced diurnal modulation of the precipitation (tickmarks on abscissa correspond to 0800 LST). Information concerning the *timing* of rainfall maxima has been extracted from Fig. 3 and is presented in Fig. 4. Most rainfall over the mountains occurred during the afternoon and evening hours (79% of the peaks exceeding 1 mm per 6 h were at 1400 and 2000 LST), consistent with the expected effects of sea-breeze forcing. Rainfall on the west coastal plains was shifted to slightly earlier times, with 75% of the peaks occurring at 0800 and 1400 LST. There is some evidence to indicate that the earlier occurrence of rain near the coast is, in part, attributable to frequent instances of convergence of the nighttime land breeze with the southwesterly low-level monsoon flow, which generates coastal convection during the early morning hours. Another mechanism for coastal convergence may involve blocking and the development of stagnation flow upwind of the island (Smolarkiewicz et al. 1988). Indeed, Doppler radar data collected on the northwest coast of Taiwan indi-

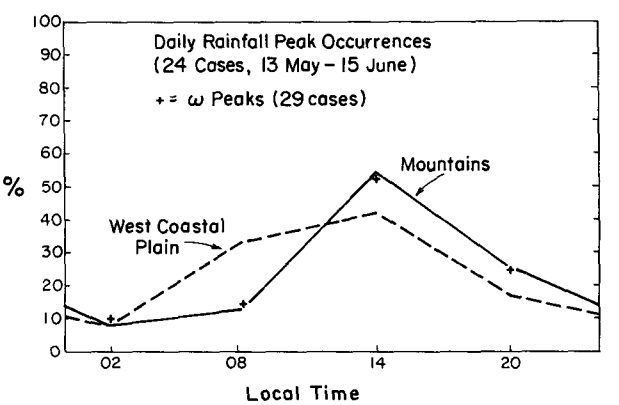

FIG. 4. Frequency distribution of daily rainfall peak occurrences based on 6-h totals for the mountains and the west coastal plain. Pluses indicate frequency distribution of ω peaks from Fig. 6.

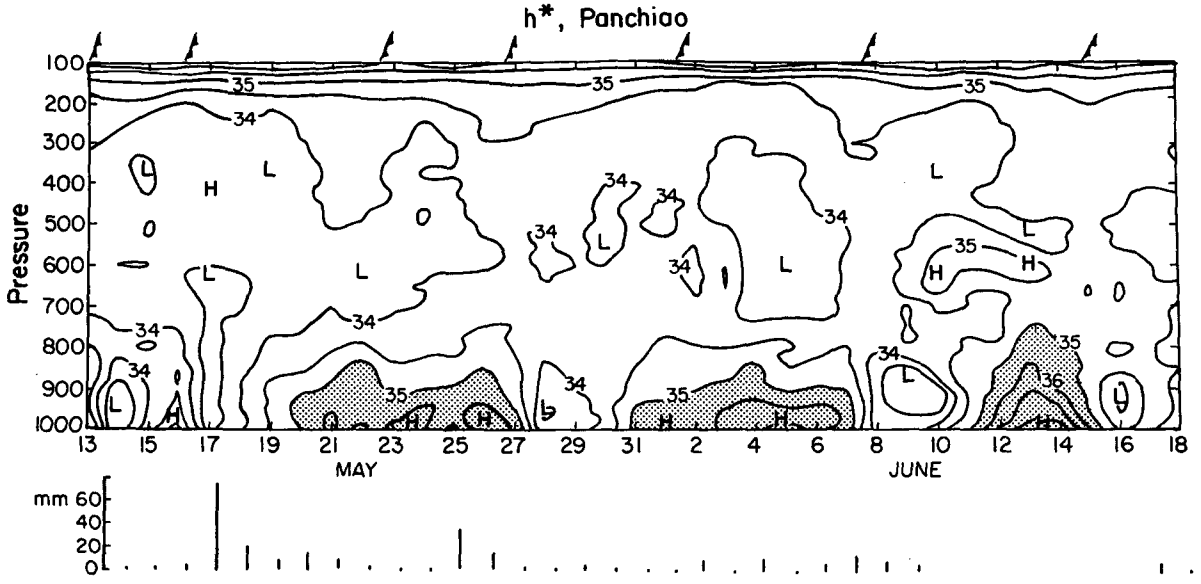

FIG. 5. Time series of moist static energy h^* ($\times 10^4$ m^2 s^{-2}) at Panchiao during the special observing period. Values exceeding 35 are shaded. Times of cold-front passage are indicated by symbols at top. Daily rainfall totals (mm) at Panchiao are shown at bottom. Tick marks on abscissa correspond to 0800 LST.

cated frequent formation of convective bands offshore during the early morning hours, followed by subsequent propagation onshore and dissipation after sunrise (D. Parsons, personal communication). In addition, there may also be a suppression of coastal plain precipitation in the late afternoon due to compensating subsidence from deep convection over the interior mountains as has been observed elsewhere on tropical islands (e.g., Malkus 1955).

For the entire SOP, the total rainfall averaged separately over the mountain and coastal plain areas was 393 and 238 mm, respectively. Since the mountain total is greater, it is evident from Fig. 4 that for the polygon as a whole there is a clear preference for the maximum rainfall amounts to occur in the afternoon and evening hours. This information will be used to interpret the vertical motion for the entire polygon area.

2) VERTICAL MOTION

Before presenting vertical motion results, a time series of saturation moist static energy h^* at Panchiao on the northern end of Taiwan is shown in Fig. 5. Also indicated are daily rainfall totals at Panchiao and times of occurrence of cold-front passages at the northern tip of Taiwan. It can be seen that the TAMEX SOP is characterized by three primary ~1-week periods of low-level conditional instability, associated with southwest monsoon flow, interspersed by 3–5-day periods of stable conditions, each associated with the passage of a cold front. Important for later discussion, it is noted that rainfall at Panchiao occurred during both conditionally unstable and stable periods.

In Fig. 6, a time series of vertical motion for the entire TAMEX SOP is shown. Indicated below each panel in the figure are the duration of the conditionally unstable periods at Panchiao (dashed line) and a time series of the entire polygon rainfall. The timing of conditional instability at Panchiao can be considered to roughly apply to the entire polygon. Several patterns of vertical motion are evident. First, it is apparent that during the periods of conditional instability, the peaks in upward motion are generally in the mid- to upper troposphere, whereas during stable periods, upward motion peaks are confined to the lower troposphere. This finding is consistent with the expected deep convection at times of conditional instability and the absence of such convection at other times. The prominent low-level peaks between 650 and 750 mb during the stable periods are typically associated with stratiform precipitation forced by frontal and/or orographic effects.

Second, there is a regular diurnal pattern to the vertical velocity with upward motion predominantly occurring in the afternoon and evening (76% of the daily peaks were at 1400 and 2000 LST) and downward motion generally at night or in the early morning (0200 and 0800 LST). This pattern resembles very closely the diurnal variation of rainfall. To see this correspondence, we have plotted the frequency distribution of ω peaks from Fig. 6 along with the rainfall distribution in Fig. 4. The timing of ω and the mountain rainfall peaks agree well, giving some confidence to compu-

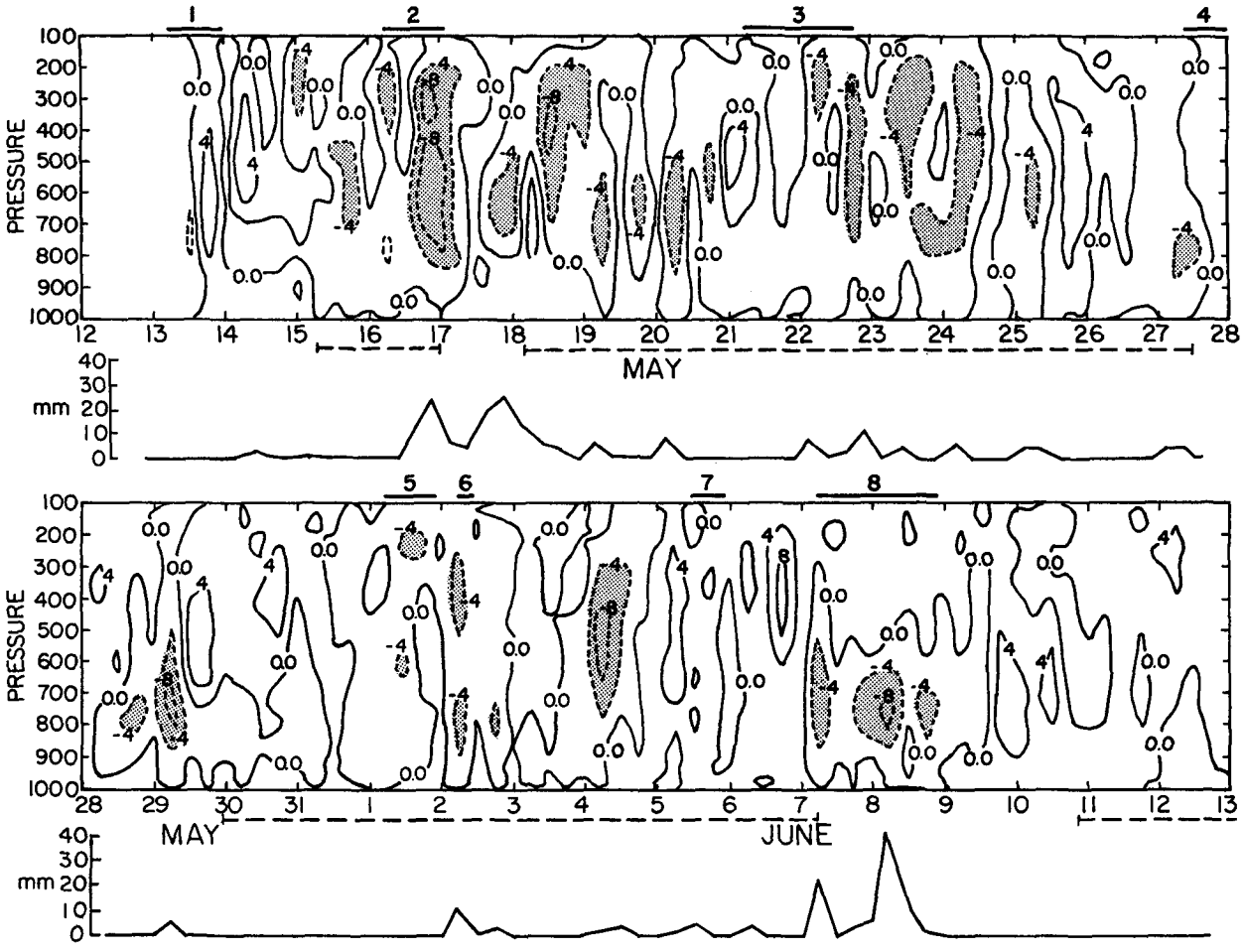

FIG. 6. Time series of ω (μb s^{-1} or 0.1 Pa s^{-1}) during the special observing period. Strong upward motion areas are shaded. Intensive observing periods (IOPs) 1–8 are indicated at top. Horizontal dashed line denotes periods of conditional instability at Panchiao (from Fig. 5). Time series of average rainfall (mm) over the sounding polygon is shown at the bottom of each panel. Tick marks on abscissa correspond to 0800 LST.

tations of the vertical motion field over Taiwan, since the mountain contribution is a dominant part of the total polygon rainfall.

The night and early morning downward motion peaks are considerably stronger than that expected from radiatively driven subsidence alone. Enhanced downward motion at these times may be a consequence of the combined effects of the island land breeze, the mountain drainage flows, and the evaporation and sublimation of precipitation from the previous evening's convection over the island. The latter possibility will be explored further when considering heat and moisture budgets for 24 May (section 3c).

It can be seen from Fig. 6 that the periods of heaviest rainfall generally correspond to times of strong upward motion. However, there are a few instances when strong upward motion occurred with little to no rainfall, most notably on 29 May and 4 June. The first case (29 May) exhibits a low-level vertical motion peak and occurs during a stable period. It can be traced to anomalously strong westerly winds at low levels at Makung in association with a front over southern Taiwan. The second (4 June) appears to be a result of convection just east of the island adversely affecting the winds at Panchiao.

Time series for Q_1 and Q_2 for the entire SOP have been prepared but will not be shown since they closely resemble that for ω (Fig. 6). However, Q_1, Q_2, and ω profiles corresponding to the 17–18 May and 7–8 June heavy rain events during the SOP will be presented in the next subsection.

The validity of heat and moisture budgets can be independently checked by comparison of the integrated Q_1 and Q_2 with surface measurements of rainfall, sensible heat flux, and evaporation (Yanai et al. 1973). This procedure has been carried out for the entire SOP and has met with limited success, although the detailed results are not presented here. The integrated Q_2 and surface precipitation generally correlate well, but there are exceptions. Obviously the 29 May and 4 June cases

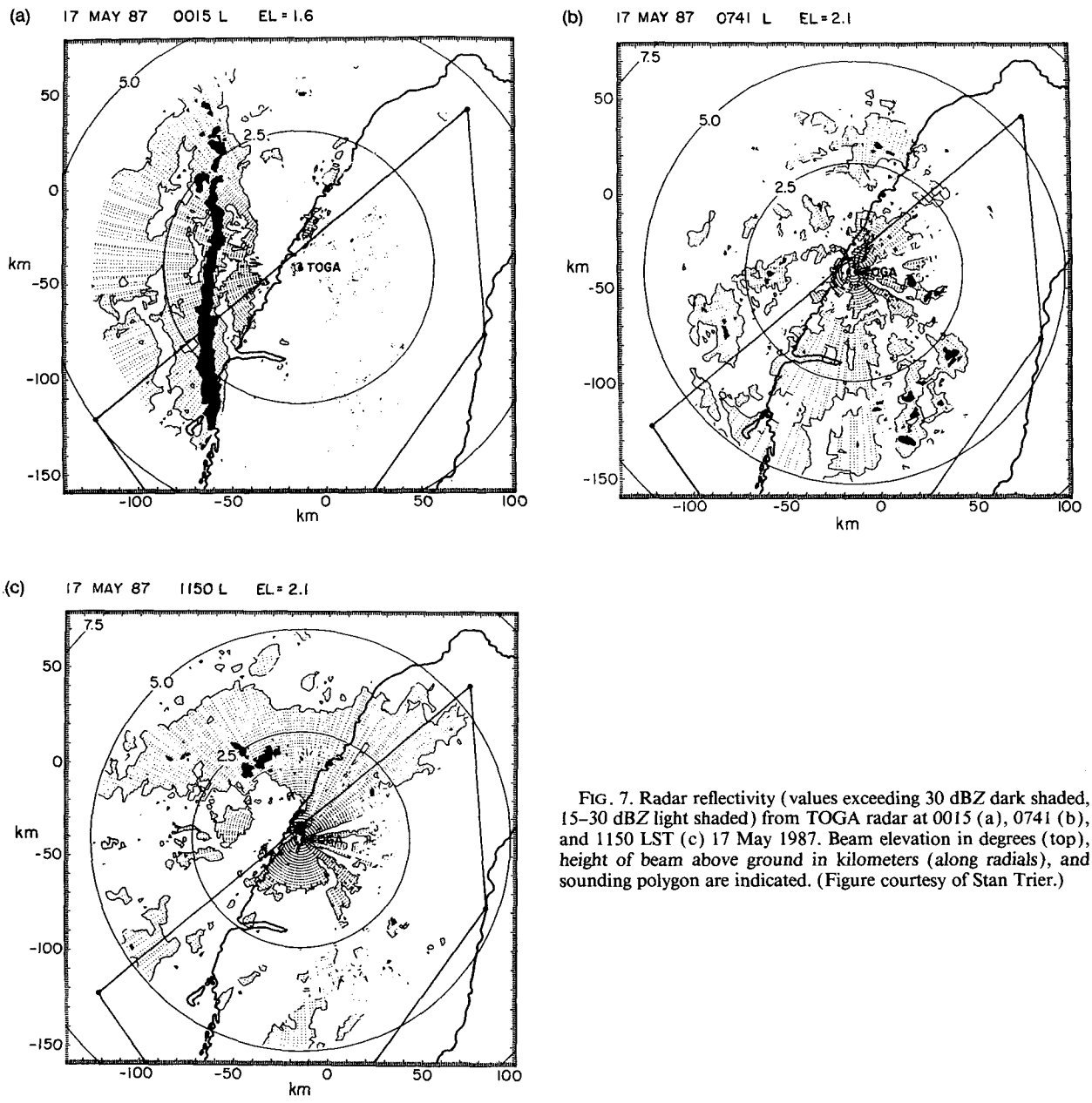

FIG. 7. Radar reflectivity (values exceeding 30 dBZ dark shaded, 15–30 dBZ light shaded) from TOGA radar at 0015 (a), 0741 (b), and 1150 LST (c) 17 May 1987. Beam elevation in degrees (top), height of beam above ground in kilometers (along radials), and sounding polygon are indicated. (Figure courtesy of Stan Trier.)

discussed above are two important exceptions. In general, we attribute the disagreements at individual times to inadequacies in both the sounding data network and the precipitation measurements, as well as the occasional contamination of individual soundings by localized transient effects (e.g., thunderstorms at a station). However, the total surface precipitation for the entire SOP determined from the integrated moisture budget, 343 mm (assuming a 2.5 mm day^{-1} surface evaporation taken from a study over a similarly vegetated surface; Johnson 1976), agrees well with the surface station total of 308 mm. The agreement is exact for an assumed 1.5 mm day^{-1} surface evaporation. Unfortunately, a precise value of evaporation over this complex land surface area is difficult to determine.

b. Intensive observing periods 2 and 8 (17–18 May and 7–8 June)

Here we examine vertical motion and heating and moistening distributions for the two major rainfall episodes during the TAMEX SOP. As already indicated, both were characterized by two rainfall peaks separated by 24 h.

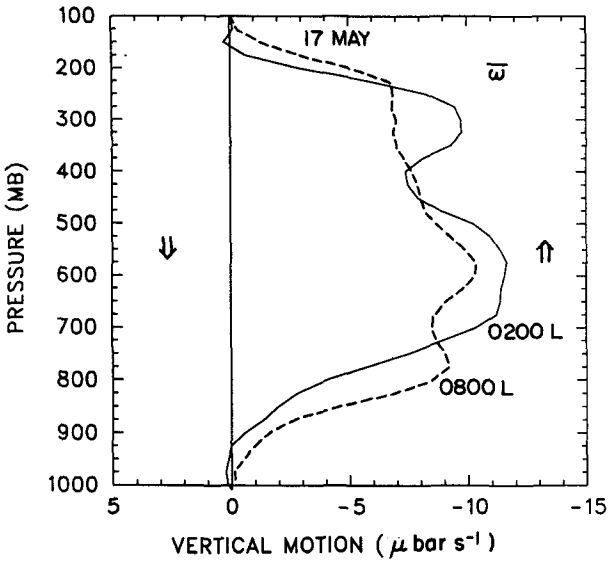

FIG. 8. Polygon-averaged vertical motion $\bar{\omega}$ (μb s^{-1}) at 0200 (solid) and 0800 LST (dashed) 17 May.

1) 17–18 MAY CASE

A sequence of plan-position indicator (PPI) scans from the NOAA TOGA radar at 0015, 0741, and 1150 LST is shown in Fig. 7. In Fig. 7a, a prefrontal north–south squall line approximately 200 km in length can be seen approaching the northwest coast of Taiwan, having an eastward speed of 16 m s^{-1}. The storm contained a trailing stratiform precipitation region extending to the rear of the leading convective line and a rear inflow jet at the base of the stratiform cloud (Wang et al. 1990), much like squall lines observed elsewhere in the tropics and midlatitudes (Houze et al. 1989). The reader is referred to Wang et al. (1990) for a documentation of the kinematic and precipitation structure of this squall line. The maximum reflectivity and echo tops in the convective line observed by the NCAR research radar were 47 dBZ and 14.6 km (130 mb), respectively (Parsons and Trier 1989). Over the next 7 h, precipitation moved inland such that by 0741 LST (Fig. 7b) widespread light rain was occurring over the coastal regions and deep convection was occurring over the central mountains. By this time a cold front had moved to the southern portion of the radar domain, reaching central Taiwan by 0800 LST and southern Taiwan by 2000 LST. The predominance of convective rainfall over the island up until 0800 LST is confirmed by a conventional weather station and the hourly raingage network data, as well as the radar analyses of Wang et al. (1990). Approximately 4 h later at 1150 LST (Fig. 7c), stratiform precipitation enveloped much of the region following a cold-frontal passage.

Shortly after 1200 LST, all research Doppler radars terminated operation. Consequently, research radar information regarding the second rainfall peak at 0800 LST is not available. Most of the precipitation in the polygon area at this time was associated with postfrontal overrunning, as the surface cold front was positioned at the southern tip of Taiwan at 0800 LST (not shown). Examination of hourly precipitation amounts over the region indicates light, uniform rainfall over most of the entire area, with 2–6 mm h^{-1} rates typical of the coastal plain and 4–10 mm h^{-1} rates of the mountains

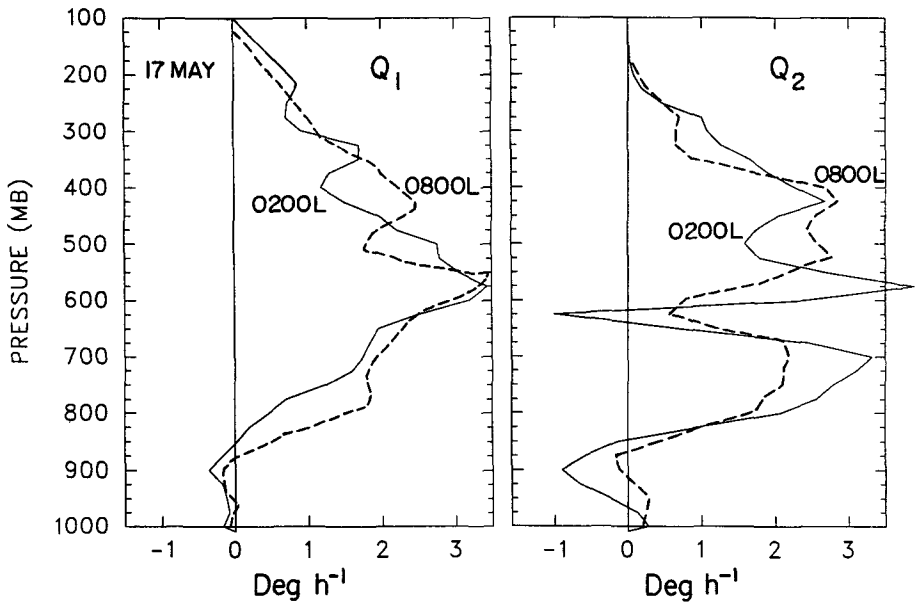

FIG. 9. Profiles of Q_1 and Q_2 (°C h^{-1}) at 0200 (solid) and 0800 LST (dashed) 17 May.

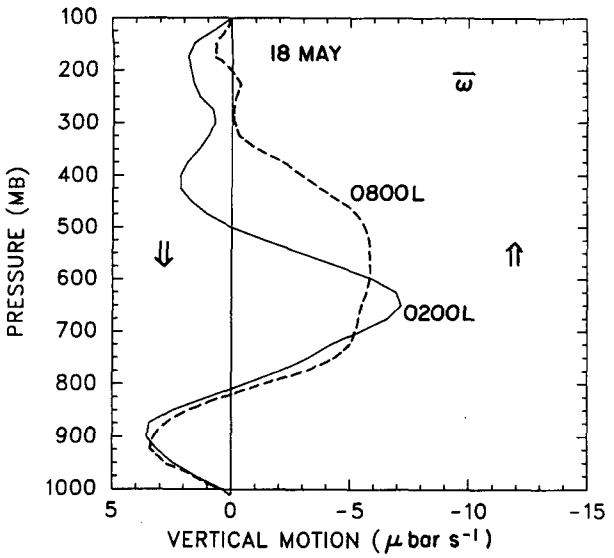

FIG. 10. As in Fig. 8, except for 18 May.

on 18 May. Thus, the rainfall at this time was stratiform in character and quite distinct from highly convective structure early on 17 May.

In Fig. 8, the vertical motion at 0200 and 0800 LST 17 May is shown. Deep upward motion is evident with peaks near 600 and 300 mb, consistent with the Doppler radar observations of deep convection within the polygon area at these times. There is some indication of a weakening of the deep convection (the upper-level peak) at 0800 LST. It is encouraging to note that while deep convection at the earlier time is not well centered within the polygon (Fig. 7a), there is nevertheless a consistency between the radar and vertical motion fields.

Profiles of Q_1 and Q_2 at 0200 and 0800 LST are shown in Fig. 9. Heating Q_1 has primary peaks near 550 mb, whereas Q_2 exhibits two peaks, one at upper levels (broadly between 400 and 550 mb) and the other at low levels near 700 mb. The separation between the Q_1 and lower Q_2 peaks was shown by Luo and Yanai (1984) to be an indicator of deep convection, which is confirmed in this case. But also present in our situation is an upper level Q_2 peak roughly coincident with that of Q_1, suggestive of a contribution from stratiform precipitation. Indeed, in this case we observe a mixture of convective structures ranging from cellular convection to stratiform precipitation, the latter being associated with a squall line and then, later, frontal overrunning and orographic effects. Johnson and Young (1983) have noted that Q_1 and Q_2 for mesoscale anvils associated with tropical squall systems have nearly coincident peaks in the upper troposphere. The squall-line trailing stratiform cloud may have contributed to the upper-level peaks in our case.

Interestingly, a midtropospheric minimum in Q_2 (near 625 mb) is present at both times. Such a structure has been attributed by Johnson (1984) and Esbensen et al. (1988) to the coexistence of both convective and stratiform clouds in a region, with the lower drying peak caused by deep convective clouds and the upper peak by upper-level stratiform clouds. This explanation is certainly consistent with the observations of two types of cloud systems in the region. However, Dudhia and Moncrieff (1987) and Lafore et al. (1988) alternatively

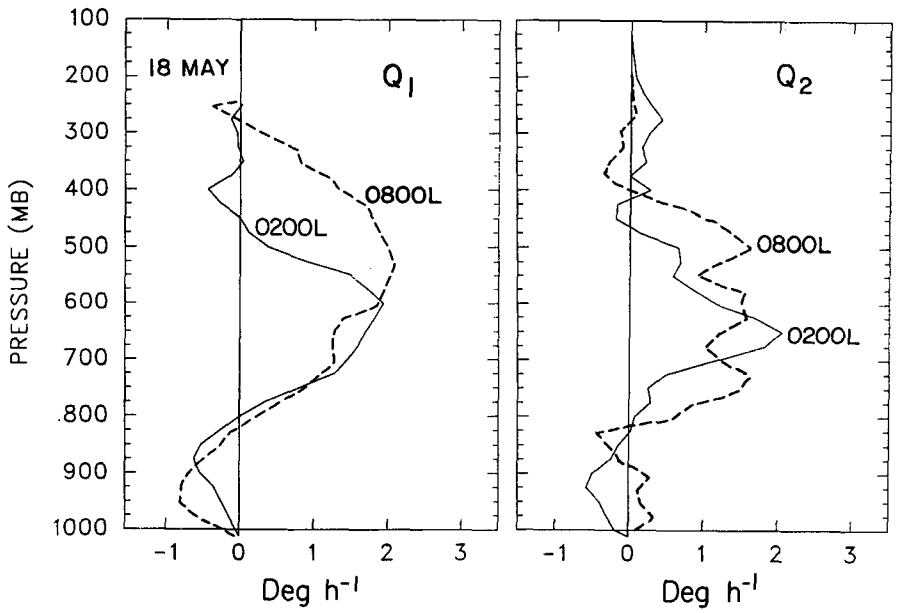

FIG. 11. As in Fig. 9, except for 18 May.

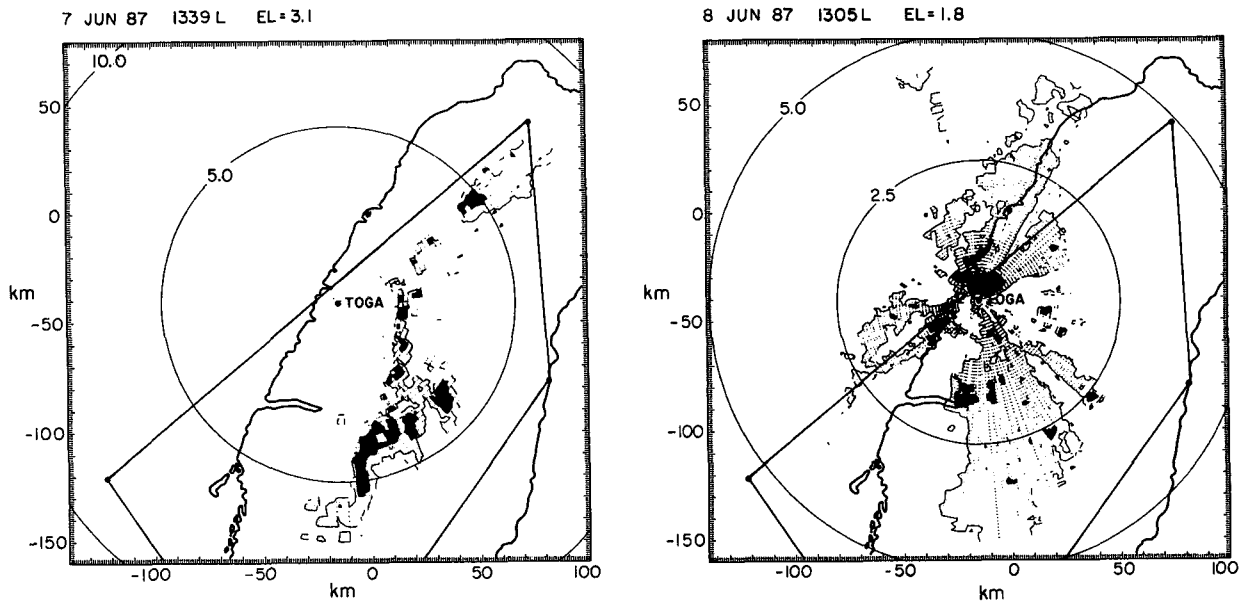

FIG. 12. Radar reflectivity (values exceeding 30 dBZ dark shaded, 15–30 dBZ light shaded) from TOGA radar at 1339 LST 7 June (a) and 1305 LST 8 June (b); rest as in Fig. 7. (Figure courtesy of Stan Trier.)

argue that this double-peak structure may be a result of eddy flux convergence of water vapor in the deep convective towers. This process may also be occurring, but we are unable to discern to what extent from the available data.

Vertical motion profiles at 0200 and 0800 LST 18 May are presented in Fig. 10. The pattern is distinctly different from that 24 h earlier with upward motion in the midtroposphere (above 800 mb) and downward motion below. Correspondingly, the Q_1 and Q_2 profiles show heating and drying in the midtroposphere and cooling and moistening below (Fig. 11). This structure is consistent with the existence of stratiform precipitation, where the stratiform cloud layer exists in the midtroposphere and rainfall evaporation dominates in the lowest levels. It is similar to that determined for tropical mesoscale stratiform cloud systems (e.g., Johnson and Young 1983), except that the peaks at both upper and lower levels are shiftward downward in this case. The lower maxima are consistent with the presence of frontal and/or orographically generated stratiform precipitation, in contrast with the tropics where detrainment from deep cumulonimbus plays an essential role.

2) 7–8 JUNE CASE

NOAA TOGA radar PPI scans at 1339 LST 7 June and 1304 LST 8 June are shown in Fig. 12. A pattern characteristic of deep convection can be seen over the mountains on the 7th (Fig. 12a). Maximum tops were near 17 km and reflectivities approached 60 dBZ at this time (Parsons and Trier 1989). Nearly 24 h later (Fig. 12b), a cold front was passing through the TOGA radar site (Trier et al. 1990). The precipitation at this time was much more widespread with a considerable stratiform component, although imbedded convection, having relatively shallow tops (to 7–8 km; Trier et al. 1990), also existed over portions of the domain.

The vertical motion profiles at 1400 LST 7 and 8 June are shown in Fig. 13. The profile on the 7th shows

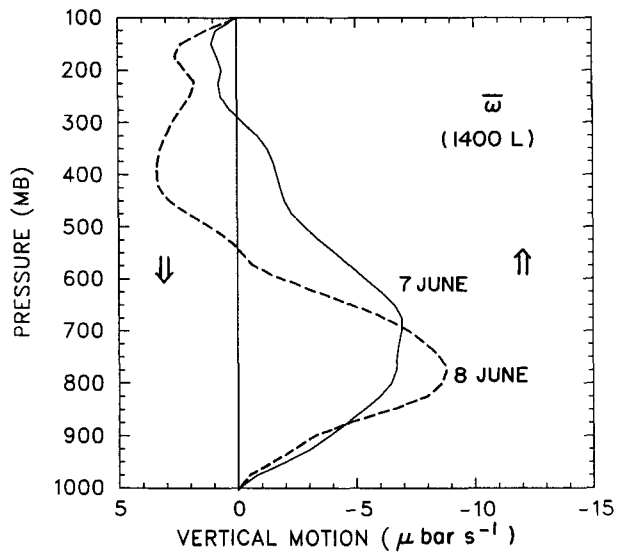

FIG. 13. Polygon-averaged vertical motion $\bar{\omega}$ (μb s^{-1}) at 1400 LST 7 (solid) and 8 (dashed) June.

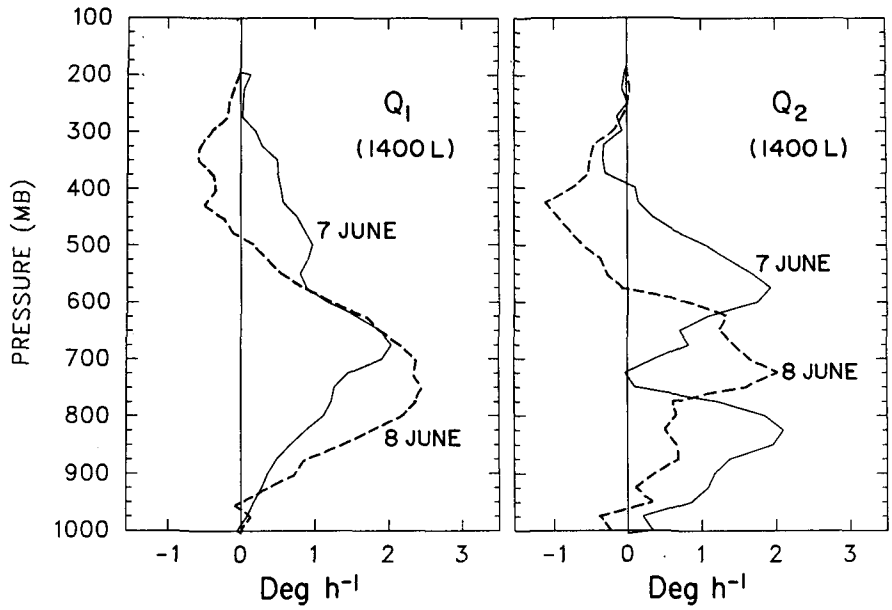

FIG. 14. Profiles of Q_1 and Q_2 (°C h^{-1}) at 1400 LST 7 (solid) and 8 (dashed) June.

upward motion to 300 mb, although the peak is not as high as might be expected considering the deep convection in the region at this time. It may be that this profile is reflective of building convection around sounding release time (approximately 45 min prior to 1400 LST) and that the strong divergence aloft indicative of deep convection is not yet present at this time at the island rawinsonde sites. (The deep convection is short-lived and therefore not evident in ω computed 6 h later.) On 8 June, 24 h later, upward motion extended only to 550 mb with sinking motion above. The confinement of upward motion to low levels is confirmed independently by an EVAD (extended velocity–azimuth display; Srivastava et al. 1986) analysis by Trier et al. (1990) in the vicinity of the cold front along the northwest coast of Taiwan. Trier et al. show that the cold front was very shallow (~1.0–1.5 km deep) and behaved much like a density current with upward motion confined to the lower troposphere along and to the rear of its leading edge.

The Q_1 and Q_2 profiles on 7 June (Fig. 14) contain a signature suggestive of deep convection: a single peak in Q_1 and a double peak in Q_2. The absence of stratiform precipitation at this early stage of the convection (Fig. 12a) supports the contention by Dudhia and Moncrieff (1987) and Lafore et al. (1988) that a double peak in Q_2 can be created by convergence of eddy moisture flux in deep convective towers. Only a single positive Q_2 peak occurred on 8 June, however, and it was coincident with the Q_1 peak, suggestive of stratiform precipitation (Luo and Yanai 1984).

The region of negative Q_1 and Q_2 (cooling and moistening) aloft near 400 mb on 8 June may be indicative of sublimation at these levels in connection with a "feeder–seeder" type process (e.g., Matejka et al. 1980). While the existence of some conditional instability at upper levels at this time (Fig. 5) supports the possibility of generating cells aloft producing feeder precipitation, the absence of heating in the layer above suggests, assuming this explanation to be valid, that the ice must have been advected into the polygon area. Satellite data (not shown) indicate the existence of substantial cirrus upstream of the region as a possible source.

c. Undisturbed period (24–26 May)

In this section we examine the basic characteristics of sea and land breezes for a 3-day period when synoptic-scale influences were minimal. Such conditions were difficult to find during TAMEX, as disturbed weather associated with the Mei-Yu frequently affected the Taiwan area. A regular cycle of sea and land breezes was observed at coastal stations on 24–26 May. The primary cloudiness on these days was associated with afternoon thunderstorms over the interior. Since this period was undisturbed, research radars were not activated to document the convective development.

1) PRECIPITATION

Daily precipitation totals over Taiwan for 24, 25, and 26 May are indicated in Fig. 15. The rainfall on these days occurred predominantly during the late-morning and early-afternoon hours. The spotty character to the rainfall indicates that the precipitation was

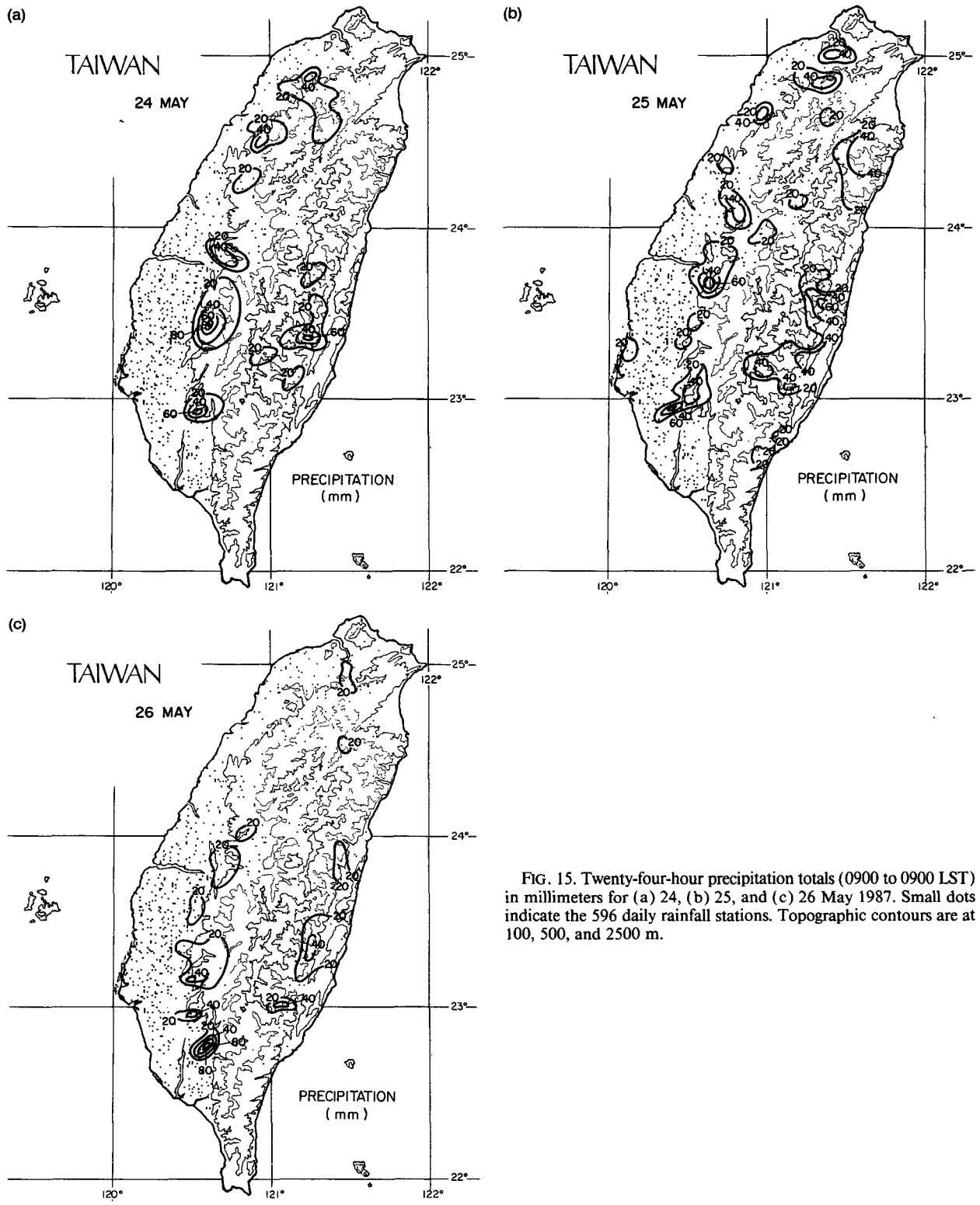

FIG. 15. Twenty-four-hour precipitation totals (0900 to 0900 LST) in millimeters for (a) 24, (b) 25, and (c) 26 May 1987. Small dots indicate the 596 daily rainfall stations. Topographic contours are at 100, 500, and 2500 m.

convective in nature. The thunderstorms were most numerous on the 24th and 25th (Figs. 15a and 15b), diminishing considerably over the northern half of the island on the 26th (Fig. 15c) as drier air aloft moved over that region. A very interesting behavior of the convection on these 3 days was a preference for

convection to occur at 100–500 m rather than over the high mountainous interior. Considering that most of this precipitation occurred in the afternoon in association with the sea breeze, a possible explanation for this pattern is a triggering of convection where the inflowing sea-breeze air first meets an abrupt rise in the topography.

2) Timing of sea and land breezes

The time of onset of the sea breeze on each day is shown in Fig. 16. During this 3-day period, the low-level flow impinging on the island (below 3 km) was south to southwesterly, as indicated at the adjacent island stations in Fig. 16. Along the west coastal plain, the sea-breeze onset was typically around 0900 LST, advancing inland to the base of the mountains during the next hour. On the east coast, the time of onset of onshore flow was more variable, perhaps as a result of irregularities in the flow associated with vortex shedding downstream of the island barrier (Smolarkiewicz et al. 1988). Earlier onset on the east coast was expected due to the east-facing mountain slopes and, in fact, did occur in a few instances.

The time of onset of offshore flow is shown in Fig. 17. Generally, offshore flow commenced during the evening hours (near sunset); however, considerable variability existed as a result of outflows from afternoon thunderstorms. On some nights at some stations, the transition to offshore flow was not observed at all. In most of these cases the surface wind became calm.

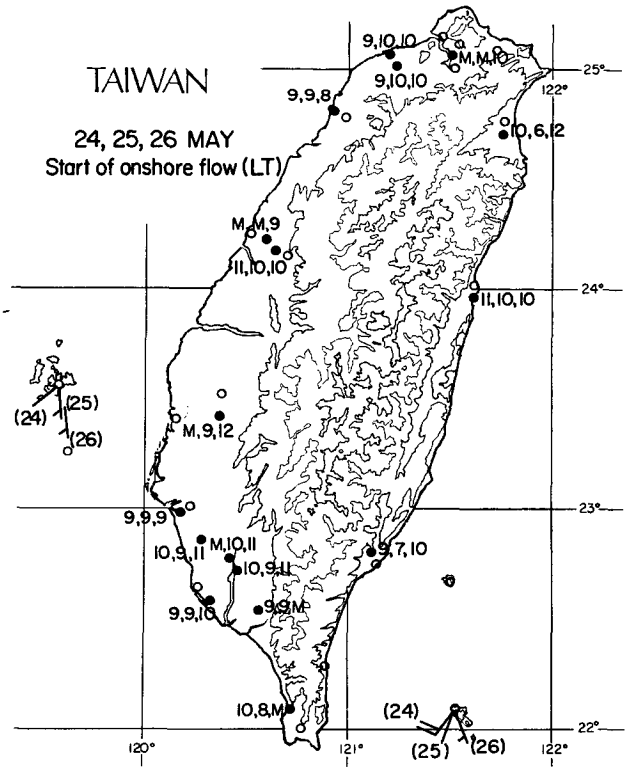

FIG. 16. Time of onset of onshore flow (LT = local time; 9 = 0900 LST, etc. for 24, 25, and 26 May). Surface winds at 0900 LST at two nearby islands are also indicated for the 3 days. At some stations on some days no transition was observed (designated by M).

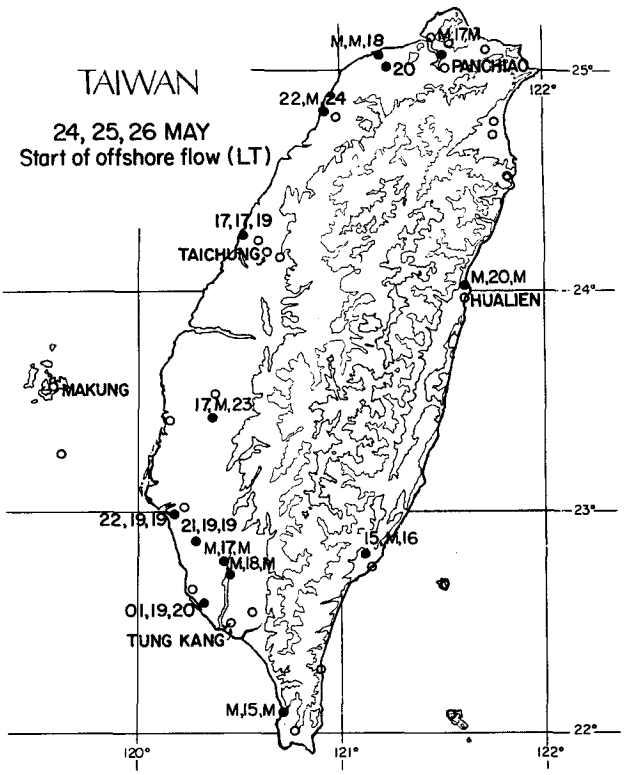

FIG. 17. As in Fig. 16, except for offshore flow. The four polygon sounding sites and a fifth sounding site, Taichung, are indicated.

3) Boundary-layer structure

The TAMEX sounding sites (Fig. 17) were not necessarily positioned for optimal determination of sea- and land-breeze structures. Panchiao is situated in somewhat of a valley approximately 20 km inland from the north coast, and the low-level flow is likely influenced at times by local terrain features. Taichung, approximately 20 km inland on the west coastal plain, is in an ideal position for study of the sea and land breezes; however, there were considerable sounding equipment difficulties at that site. The two other island sounding stations, Tung Kang and Hualien, are very near the coastline. Soundings from these stations during the SOP were released at 0200, 0800, 1400, and 2000 LST. Unfortunately, this time resolution is not sufficient to capture the growth of the mixed layer during the morning hours. Barring contamination by precipitation, however, the 1400 LST sounding should provide evidence of a fully developed mixed layer on clear days at the inland stations. Three-hourly soundings

were obtained during IOPs; however, these soundings were taken (almost by definition) in highly disturbed environments, so they cannot be used in this study of the undisturbed boundary layer.

In Fig. 18, dry static energy $s\ (=c_pT+gz)$ and specific humidity q are shown at 0800 and 1400 LST 24 May at Panchiao. The 1400 LST sounding depicts quite well the development of a mixed layer to near 820 mb (1.8 km) in the afternoon. Specific humidity is not well mixed, as is common over land, although there appears to be a general moistening (by 2–3 g kg^{-1}) at most levels in the mixed layer as the sea breeze brings ashore moister air during the afternoon. A turning of the winds to a northerly or onshore direction is observed throughout most of the mixed layer during the afternoon. Winds at the lowest levels are undoubtedly influenced by local river basin circulations at Panchiao and a 700-m mountain approximately 10 km north of the station.

Similar mixed-layer development is evident at Taichung (Fig. 19). Although there is an instrument error at this station yielding excessive warming above the boundary layer, this set of soundings indicates mixed-layer development to near 850 mb or 1.5 km. In this instance, the depth of the mixed layer is difficult to determine precisely; however, the turning of the wind to an onshore northwesterly direction below 850 mb strongly suggests a penetration of the sea breeze (and mixing from the surface) to this depth. A moistening is again present in the mixed layer, but also appears to extend above the mixed-layer top. It is suspected that the moistening above the mixed layer is due to the ascent of the balloon into a shallow cloud.

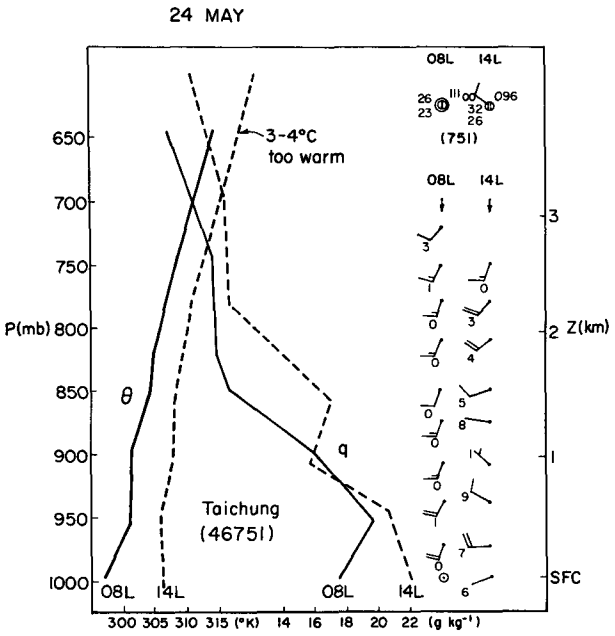

FIG. 19. Potential temperature θ (K) and specific humidity q (g kg^{-1}) at 0800 and 1400 LST 24 May at Taichung.

Observations from the east coast of the island at Hualien, where virtually no coastal plain exists (as mountains descend abruptly to the ocean), indicate boundary-layer warming and moistening during the afternoon and an absence of a well-mixed structure (Fig. 20). The wind profiles in Fig. 20 show the development of an easterly onshore flow in the afternoon extending to

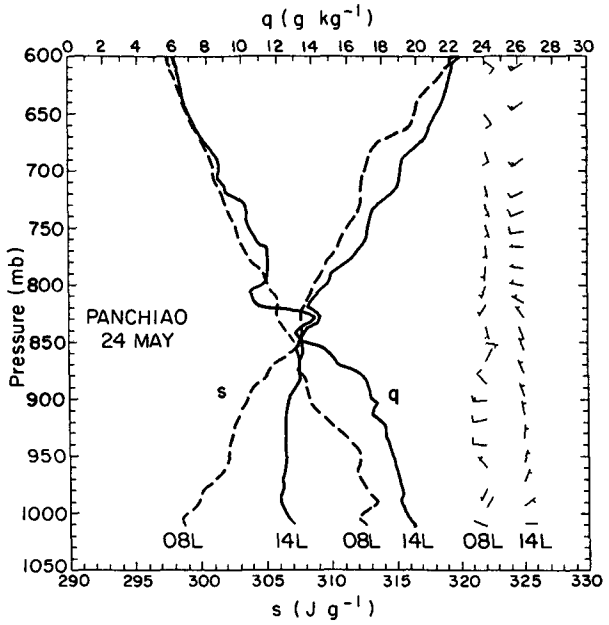

FIG. 18. Dry static energy s (J g^{-1}), specific humidity q (g kg^{-1}), and winds at 0800 and 1400 LST at Panchiao on 24 May.

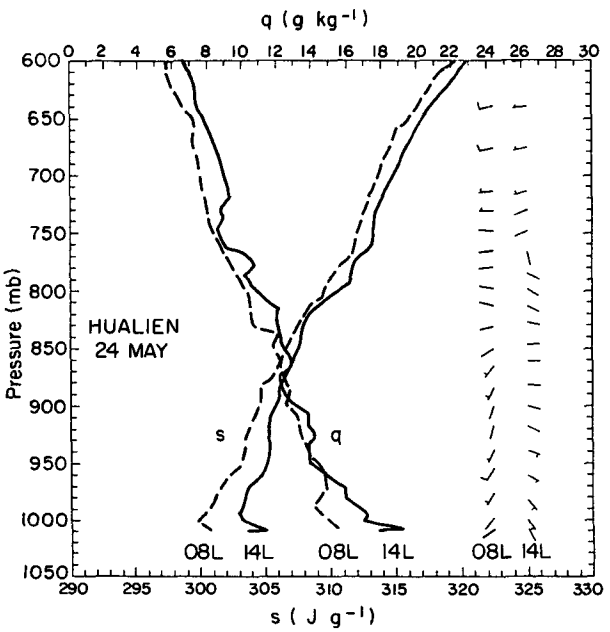

FIG. 20. As in Fig. 18, except for Hualien.

nearly 750 mb or 2.5 km. The horizontal advection of potentially cooler air from the ocean over the narrow coastal strip during the afternoon sea breeze is likely to contribute to the somewhat stably stratified boundary layer (above the surface superadiabatic layer) at Hualien. While attributing the afternoon onshore flow to island thermal forcing, it is clearly possible that circulations around the island barrier itself may be influencing the local winds at Hualien. As in the other cases, some low-level moistening due to the sea breeze is also observed at Hualien.

4) Heating and moistening distributions

Vertical motion for 24–26 May has already been shown in Fig. 6. A clear diurnal cycle is evident during this time period with maximum upward motion in the afternoon (1400 LST) on each day and generally downward motion at night. The afternoon upward motion progressively weakened through the period. The pattern of vertical motion is consistent with the observations of considerable thunderstorm activity over the interior during the afternoon of the 24th, somewhat less on the 25th, and suppressed activity on the 26th. The atmosphere became disturbed after the 26th, and the earlier diurnal pattern of vertical motion was disrupted.

The diurnal cycle of Q_1 and Q_2 on 24 May is illustrated in Fig. 21. Heating and drying developed at low levels several hours after sunrise (0800 LST) in association with developing convection and extended throughout the entire troposphere in the afternoon (1400 LST). The maximum heating occurred at very high levels (between 200 and 250 mb), and there was a distinct separation between the Q_1 and Q_2 peaks, indicative of deep convection. At 2000 LST, the heating weakened at upper levels and converted to cooling below the mountain crest. Similarly, drying aloft and moistening below is seen in the Q_2 profile. The structure of the Q_1 and Q_2 profiles at 2000 LST is characteristic of that observed within the stratiform regions of mesoscale convective systems (Houze 1982; Johnson and Young 1983). The latter studies have related the heating at high levels to condensation and freezing in the stratiform cloud aloft and the cooling below to precipitation evaporation and melting.

Finally, at 0200 LST 25 May, Q_1 converted to cooling above 700 mb. This deep layer of cooling at night is often present at other times and typically extends to near the surface (although not in this case). It is presumed to be a consequence of evaporation of cloud debris from the convection that occurred earlier in the afternoon and evening over the island. This conclusion is supported by the negative Q_2 (moistening) observed from 250 to 600 mb. (The drying below 600 mb, however, has no obvious explanation.) Radiative cooling might also contribute to the negative Q_1, but the cooling is too large and over too deep a layer to be attributed solely to radiative effects (Webster and Stephens 1980).

4. Summary, discussion, and conclusions

In this study we have examined the characteristics of precipitating cloud systems over Taiwan during the 1987 Mei-Yu TAMEX period. The primary findings are the following:

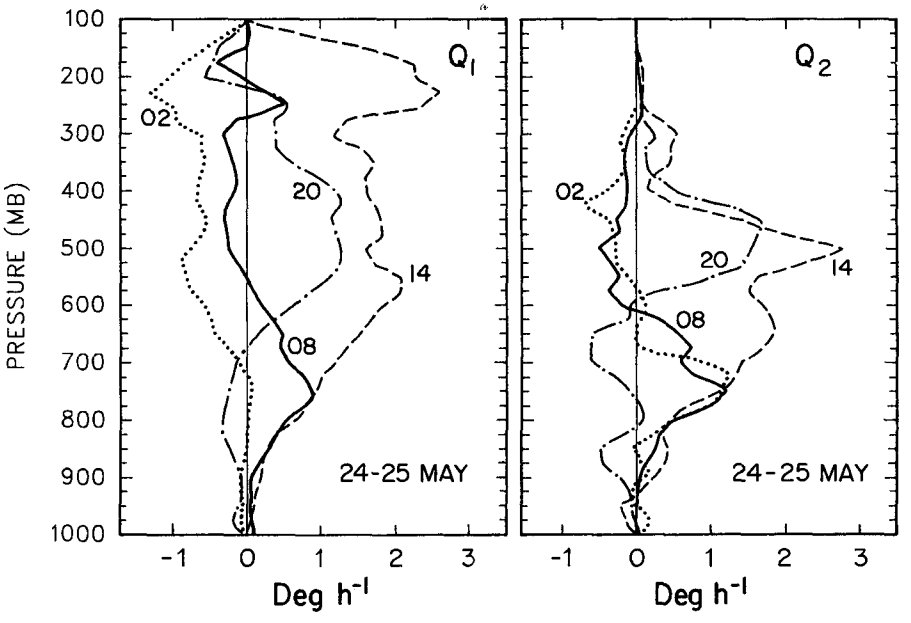

FIG. 21. Profiles of Q_1 and Q_2 (°C h^{-1}) at 0800, 1400, and 2000 LST 24 May and 0200 LST 25 May.

1) Heavy precipitation over Taiwan during the 1987 Mei-Yu consisted of both convective and stratiform components. During periods of conditional instability, deep convective rainfall predominated, although in some instances it possessed associated stratiform precipitation components as has been observed elsewhere in the tropics (e.g., Leary and Houze 1979; Houze et al. 1981). The periods of conditional instability were interrupted by stable periods and marked by the passage of cold fronts, and during both periods, a complex array of precipitation structures occurred. In one case studied, a squall line having a deep convective line and trailing stratiform region preceded cold-frontal passage, followed by stratiform precipitation connected with frontal overrunning and orographic effects. The two heaviest rainfall events over the western part of Taiwan during the TAMEX SOP were generally stratiform in character.

2) During periods of deep convection, deep upward motion was present and a separation of Q_1 and Q_2 peaks was observed (noted as a signature of deep convection by Luo and Yanai 1984). A double-peak structure to Q_2 was observed at times of deep convection, as has been noted elsewhere (Johnson 1984; Esbensen et al. 1988; Dudhia and Moncrieff 1987; and Lafore et al. 1988). The existence of a double-peak structure to Q_2 early in the convective cycle on 7 June, when only deep convection was present, supports the contention by Dudhia and Moncrieff (1987) and Lafore et al. (1988) that convergence of eddy moisture flux in deep convective towers can by itself lead to this feature. However, at other times, when both deep convection and upper-level, precipitating stratiform clouds were known to exist, double peaks in Q_2 may also have been a result of these two distinct precipitation features. When stratiform precipitation was present, the Q_1 and Q_2 peaks were nearly coincident. These findings generally support those of Luo and Yanai (1984), indicating a predominance of stratiform rainfall over the entire southern China and Yangtze regions (including Taiwan) during the Mei-Yu; however, they also suggest that in at least a portion of this region the precipitation may consist of a mixture of deep convection and stratiform components.

3) The instances of stratiform precipitation in the Taiwan area (contributing to moderate-to-heavy rain) were characterized by coincident Q_1 and Q_2 peaks in the mid- to lower troposphere (600–800 mb), as opposed to the occurrence of nearly coincident Q_1 and Q_2 peaks in Luo and Yanai (1984) at a somewhat higher level (near 400–500 mb). The lower peaks in the Taiwan area are consistent with the existence of shallow cold-frontal lifting in stable air (where gravity-current dynamics appear to be relevant; Trier et al. 1990) and stable orographic lifting. In contrast, the higher peaks farther north over southern China and the Yangtze region (Luo and Yanai 1984) may indicate the effects of large-scale ascent in baroclinic systems. Thus, it appears that in the Taiwan area, heavy rain in stable situations may depend critically on low-level forcing mechanisms.

4) The diurnal cycle is a prominent feature of precipitation on Taiwan, particularly during undisturbed periods. The characteristics of the diurnal cycle have been briefly examined for an undisturbed period from 24 to 26 May when afternoon thunderstorms occurred over the interior. Several important features have been observed.

(a) The convective precipitation that occurred on the 3 days was predominantly located between the 100- and 500-m elevations at the foothills of the interior mountains rather than over the higher elevations farther inland.

(b) The sea breeze typically began at 0900 LST along the shoreline of the west coastal plain and moved inland to the base of the interior mountain range during the next 1-h period. The land breeze commenced in the evening, but its onset was more variable (at least on 24–26 May) as a result of afternoon thunderstorms over the interior.

(c) Well-mixed layers (in potential temperature, but not specific humidity) developed on 24 May along the west coastal plain during the afternoon as the sea breeze penetrated inland. At a distance inland of 20–25 km the mixed-layer depth was 1.5–1.8 km. A pronounced moistening of the boundary layer was observed in the afternoon as the sea breeze advected moister air inland off the ocean. The boundary layer on the very narrow east coastal strip was not well mixed, but extended to a greater depth (2.5 km) as heating on the steep east slopes of the mountains drove a deep, weak sea breeze.

(d) A regular diurnal pattern of vertical motion, heating, and moistening was observed on the three days. Deep upward motion, heating, and drying occurred in the afternoon and weak downward motion, cooling, and moistening occurred at night. The upward motion in the afternoon is an indication of deep convection over the interior. Unexpectedly strong downward motion and cooling were observed at night. These features may be a combined effect of the land breeze, drainage flow, and evaporation of the previous afternoon and evening's precipitating cloud systems. The diurnal variation of heating and moistening on 24 May is consistent with that observed during the life cycle of tropical cloud clusters (Houze 1982; Johnson and Young 1983).

An intriguing observation stemming from TAMEX was that the intensity of the deep convection over the interior on some afternoons was not as great as TAMEX forecasters had expected, given the deep layer of conditional instability and warm, moist southwesterly flow. The elevated heating and (presumed) orographic lifting of the impinging flow, coupled with conditional instability and abundant moisture, suggested potentially vigorous afternoon thunderstorms over the in-

terior mountain range. While thunderstorms at times did occur, they did not always produce widespread, heavy rainfall. A possible explanation for this behavior is suggested by the work of Smolarkiewicz et al. (1988). Although orographic lifting might be anticipated with southwesterly flow impinging on the island, it is likely that this effect is minimized by blocking of much of the flow below the mountain crest in this low-Froude-number regime (Smolarkiewicz et al. 1988). Orographic lifting on these days may have been confined to near mountaintop levels. Analyses of the flow at 850 mb (not shown) indicate that the low-level flow was indeed frequently blocked. This blocking creates low-level divergence and subsidence on the upwind side of the island, which may have acted to retard convection and keep it from reaching intense levels.

At times when island heating is significant, however, the Froude number is increased and considerable orographic lifting can occur (Smolarkiewicz et al. 1988). This situation may have been the case in late June when the intensity of afternoon thunderstorms did increase, possibly as a consequence of increased heating. Additionally, however, the stronger diurnal convective cycle observed then may have been aided by the greater and deeper conditional instability that developed as a more tropical airmass characteristic of summer enveloped the island.

In this study we have investigated the diurnal cycle of precipitation only during the 1987 TAMEX SOP. Since a major flood did not occur during TAMEX, we know very little about diurnal effects in such cases. It has been determined by Chen (1985), based on 10 years of data, that about 75% of the heavy rainfall over Taiwan occurs at night. Heavy rainfall has been positively correlated with occurrences of low-level jets (Matsumoto 1972; Akiyama 1973; Chen 1983 and Chen and Yu 1988), features themselves that are known to have distinct diurnal variability (Bonner 1968). While the impact of the diurnal cycle on heavy rain is an extremely important problem, its full understanding is beyond the scope of this study. We have only made a first step in this direction by examining the diurnal cycle for the simplest situation, synoptically undisturbed conditions.

Acknowledgments. This research has been supported by the National Science Foundation, Division of Atmospheric Sciences, under Grant ATM-8711649. Computing support was provided by the Scientific Computing Division of the National Center for Atmospheric Research, which is sponsored by the National Science Foundation. We appreciate the assistance of Aubrey Schumann, Sue Chen, and Y.-H. Kuo in acquiring data, Paul Ciesielski for programming help, and Stan Trier for providing Figs. 7 and 12. The comments of two anonymous reviewers have considerably improved the manuscript.

REFERENCES

Akiyama, T., 1973: Frequent occurrence of heavy rainfall along the north side to the low-level jet stream in the Baiu season. *Pap. Meteor. Geophys.*, **24,** 379–388.

Bonner, W. D., 1968: Climatology of the low-level jet. *Mon. Wea. Rev.*, **96,** 833–850.

Chen, G. T.-J., 1983: Observational aspects of the Mei-Yu phenomenon in subtropical China. *J. Meteor. Soc. Japan,* **61,** 306–312.

——, 1985: Feasibility study of a severe regional precipitation observational and analysis experiment. Science Technology of Disaster Mitigation Program, National Science Council, Tech. Rep. 73–423, 32 pp. (in Chinese with English abstract.) [Available from the National Science Council, 2 Canton Street, Taipei, Taiwan, Republic of China.]

——, and C.-C. Yu, 1988: Study of low-level jet and extremely heavy rainfall over northern Taiwan in the Mei-Yu season. *Mon. Wea. Rev.*, **116,** 884–891.

Dudhia, J., and M. W. Moncrieff, 1987: A numerical simulation of quasi-stationary tropical convective bands. *Quart. J. Roy. Meteor. Soc.*, **113,** 929–967.

Esbensen, S. K., J.-T. Wang and E. I. Tollerud, 1988: A composite life cycle of nonsquall mesoscale convective systems over the tropical ocean. Part II: Heat and moisture budgets. *J. Atmos. Sci.*, **45,** 537–548.

Houze, R. A., Jr., 1982: Cloud clusters and large-scale vertical motion in the tropics. *J. Meteor. Soc. Japan.* **60,** 396–410.

——, S. G. Geotis, F. D. Marks and A. K. West, 1981: Winter monsoon convection in the vicinity of north Borneo. Part I: Structure and time variation of the clouds and precipitation. *Mon. Wea. Rev.*, **108,** 1595–1614.

——, S. A. Rutledge, M. I. Biggerstaff and B. F. Smull, 1989: Interpretation of Doppler weather radar displays of midlatitude mesoscale convective systems. *Bull. Amer. Meteor. Soc.*, **70,** 608–619.

Johnson, R. H., 1976: The role of convective-scale precipitation downdrafts in cumulus and synoptic-scale interactions. *J. Atmos. Sci.*, **33,** 1890–1910.

——, 1984: Partitioning tropical heat and moisture budgets into cumulus and mesoscale components: Implications for cumulus parameterization. *Mon. Wea. Rev.*, **112,** 1590–1601.

——, and D. L. Priegnitz, 1981: Winter monsoon convection in the vicinity of north Borneo. Part II: Effects on large-scale fields. *Mon. Wea. Rev.*, **109,** 1615–1628.

——, and G. S. Young, 1983: Heat and moisture budgets of tropical mesoscale anvil clouds. *J. Atmos. Sci.*, **40,** 2138–2147.

Kuo, Y.-H., and G. T.-J. Chen, 1990: The Taiwan Area Mesoscale Experiment (TAMEX): An overview. *Bull. Amer. Meteor. Soc.*, **71,** 488–503.

Lafore, J.-P., J.-L. Redelsperger and G. Jaubert, 1988: Comparison between a three-dimensional simulation and Doppler radar data of a tropical squall line: Transports of mass, momentum, heat, and moisture. *J. Atmos. Sci.*, **45,** 3483–3500.

Leary, C. A., and R. A. Houze, Jr., 1979: Melting and evaporation of hydrometeors in precipitation from the anvil clouds of deep tropical convection. *J. Atmos. Sci.*, **36,** 669–679.

Leopold, L. B., 1949: The interaction of the trade wind and sea breeze. *J. Meteor.*, **6,** 312–320.

Luo, H., and M. Yanai, 1983: The large-scale circulation and heat sources over the Tibetan Plateau and surrounding areas during the early summer of 1979. Part I: Precipitation and kinematic analyses. *Mon. Wea. Rev.*, **111,** 922–944.

——, and ——, 1984: The large-scale circulation and heat sources over the Tibetan Plateau and surrounding areas during the early summer of 1979. Part II: Heat and moisture budgets. *Mon. Wea. Rev.*, **112,** 966–989.

Malkus, J. S., 1955: The effect of a large island upon the trade-wind airstream. *Quart. J. Roy. Meteor. Soc.*, **81,** 538–550.

Matejka, T. J., Houze, R. A., Jr., and P. V. Hobbs, 1980: Microphysics

and dynamics of clouds associated with mesoscale rainbands in extratropical cyclones. *Quart. J. Roy. Meteor. Soc.*, **106,** 29–56.

Matsumoto, S., 1972: Unbalanced low-level jet and solenoidal circulations associated with heavy rainfalls. *J. Meteor. Soc. Japan,* **50,** 194–203.

Molinari, J., and S. Skubis, 1988: Calculation of consistent flux and advective terms from adjusted vertical profiles of divergence. *Mon. Wea. Rev.*, **116,** 1829–1837.

Nitta, T., 1983: Observational study of heat sources over the eastern Tibetan Plateau during the summer monsoon. *J. Meteor. Soc. Japan,* **61,** 590–605.

O'Brien, J. J., 1970: Alternative solutions to the classical vertical velocity problem. *J. Appl. Meteor.*, **9,** 197–203.

Parsons, D. B., and S. B. Trier, 1989: Taiwan Area Mesoscale Experiment: Doppler radar operations summary. NCAR Tech. Note TN-315+STR, National Center for Atmospheric Research, 333 pp. [Available from the authors at NCAR, P.O. Box 3000, Boulder, CO, 80307.]

Smolarkiewicz, P. K., R. M. Rasmussen and T. M. Clark, 1988: On the dynamics of Hawaiian cloud bands: Island forcing. *J. Atmos. Sci.*, **45,** 1872–1905.

Srivastava, R. C., T. J. Matejka and T. J. Lorello, 1986: Doppler radar study of the trailing anvil region associated with a squall line. *J. Atmos. Sci.*, **43,** 356–377.

Tao, S., and L. Chen, 1987: A review of recent research on the east Asian summer monsoon in China. *Monsoon Meteorology,* 3d ed., C.-P. Chang and T. N. Krishnamurti, Eds., Oxford University Press, 60–92.

Trier, S. B., D. B. Parsons and T. J. Matejka, 1990: Observations of a subtropical cold front in a region of complex terrain. *Mon. Wea. Rev.*, **118,** 2449–2470.

Wang, T.-C. C., Lin, Y.-J., R. W. Pasken and H. Shen, 1990: Characteristics of a subtropical squall line determined from TAMEX dual-Doppler data. Part I: Kinematic structure. *J. Atmos. Sci.*, **47,** 2357–2381.

Webster, P. J., and G. L. Stephens, 1980: Tropical upper-tropospheric extended clouds: Inferences from Winter MONEX. *J. Atmos. Sci.*, **37,** 1521–1541.

Yanai, M. S. Esbensen, and J. H. Chu, 1973: Determination of bulk properties of tropical cloud clusters from large-scale heat and moisture budgets. *J. Atmos. Sci.*, **30,** 611–627.